Investigations on Fading Scaling with Bandwidth and Directivity at 60 GHz

Diego Dupleich*, Naveed Iqbal†, Christian Schneider*, Stephan Haefner*, Robert Müller*,
Sergii Skoblikov*, Jian Luo†, and Reiner Thomä*
*Technische Universität Ilmenau, 98684 Ilmenau, Germany
Email: diego.dupleich@tu-ilmenau.de
†Huawei Technologies Düsseldorf GmbH, 80992 München, Germany
Email: jianluo@huawei.com

***Abstract*—In the present paper we analyse small-scale fading of reflections at 60 GHz using different antennas and bandwidths. The aim is to investigate the deterministic property of the channel in view of modelling and deployment of systems with larger bandwidths and higher directivity. We have investigated the scattering effect of a reflection on a wall emulating a beam-former in a NLOS condition. The results show that the distribution of the amplitudes fit better with a Rician than a Rayleigh distribution. Furthermore, we show that an increasing bandwidth and directivity increases the *K*-factor, supporting the idea of deterministic paths apart from the LOS.**

***Index Terms*—mm-Wave, fading, 5G, channel sounding, channel modelling**

I. Introduction

The large blocks of available spectrum at mm-waves seems to be a promising solution to cope with an increasing demand on instant data rates. In that regard, there is an increasing interest of the research community and industry in characterizing communications at mm-wave frequencies for the future wireless systems.

One of the differences in propagation characteristics at mm-waves is an increased free space path-loss with isotropic antennas. However, the small wavelength enables the implementation of compact high order antenna arrays to obtain the necessary gains for mitigating path-loss. For instance, communications will be mostly dominated by directive channels. Furthermore, previous measurements at mm-waves have shown a sparse spatio/temporal characteristic of the channel and a high influence of the geometry of the scenario on the propagation characteristics, [1]. This is mostly due to the presence of few strong scatterers that dominate the environment.

Moreover, there is an expectation of using larger bandwidths at mm-waves in comparison to lower frequencies. Larger bandwidths enables the resolution of multiple paths in the time domain. The combination of directivity and larger bandwidths results in more deterministic channel with less fading, Doppler, and delay spread (DS). This influences channel estimation and also the update rate of beam-forming coefficients could be reduced. Furthermore, polarization becomes also more deterministic, [2].

In the traditional narrowband channel modelling approach with omni-directional like antennas as shown in Fig. 1a, multiple path arriving with uniformly distributed strength and angle of arrival (AoA) are combined at the receiver (Rx). This combination changes during the displacement of the Rx since these paths will arrive with different phases, leading to a variation on the signal level depending on if the paths combine constructively or destructively. These variations on the signal level are known as small-scale fading, and the absolute value of the received signal tend to follow a Rayleigh distribution. This is mostly the case in non-line of sight (NLOS) scenarios. On the other hand, if one path is relatively stronger compared to the other ones, e.g., the line of sight (LOS) path, the distribution of the absolute value of the amplitude tends to follow a Rician distribution, in which the ratio of deterministic to random components is determined by the so called *K*-factor.

However, in a system applying spatial filtering by means of beam-forming or directive antennas as shown in Fig. 1b, the paths arriving from the direction in which the beam is pointing will be stronger than the other ones, recreating the same conditions for a Rician distribution, even if we are in NLOS. Furthermore, if the bandwidth of the system is increased, multiple paths are resolved in time at the Rx and they are not randomly combined any more, reducing the small-scale fade depth, [3].

Currently, in the widely used spatial channel models (SCMs) as 3GPP, WINNER II [4], COST 2100 [5], and METIS models [6], the path gain amplitudes are assumed to be Rician and Rayleigh distributed for the LOS and NLOS scenarios, respectively. These models fit very well the propagation and

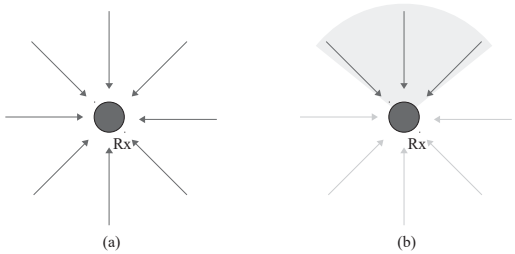

Figure 1. Effect of spatial filtering on the distribution of the arriving paths strength.

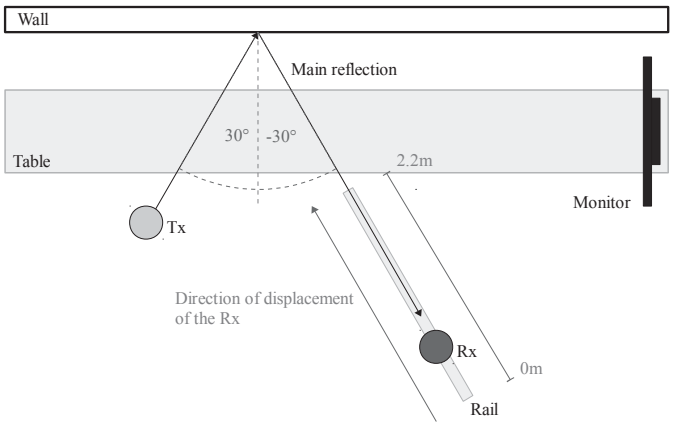

Figure 2. Top-view schematic of the measurement set-up.

system characteristics at sub-6 GHz with low directivity and short bandwidths. However, recent experimental results using directive antennas in outdoor measurements at 28 GHz with larger bandwidths (800 MHz null-to-null) have shown that the distribution of the signal envelope fits better to a Rician distribution than a Rayleigh [7], indicating the presence of strong dominant paths. In this regard, Millimetre-Wave Evolution for Backhaul and Access (MiWEBA) [8] follows a quasi-deterministic approach by superimposing a few strong deterministic paths over weaker random paths, in which the latter follow a Rayleigh distribution.

Similar investigations are presented in [9], in which the influence of bandwidth on *K*-factor and fade depth is analysed for different scatterers at 30 GHz in a lecture room scenario. In this paper, we extend those investigation to the influence of directivity and bandwidth on fading at 60 GHz. With a simple set-up addressing a specular reflection on a wall in the laboratory, we analyse the distribution of the signal amplitude for different bandwidths and directivity of antennas, looking for evidence of strong deterministic scattering effects, visible in a reduced fade depth and large *k*-factors. The results support the need of more deterministic approaches on channel modelling at mm-waves.

II. Experimental Set-up

A. Measurement Set-up

In order to study the fading characteristics at 60 GHz, we have performed measurements in a room as indicated in Fig. 2. The use of beam-forming in a NLOS condition was emulated by using directive antennas pointing to a wall in order to generate an specular reflection. Furthermore, the Rx was automatically moved along a track in $\lambda/2$ steps to investigate the variations on the signal strength during displacement. Besides the reflection in the wall, there are other scatterers as a monitor on the side, shown in Fig. 3, which influences the channel when using low directive antennas. However, these scatterers remain almost invisible with high directive antennas since they are in a different pointing direction.

Table I
Antenna and bandwidths used during the experiments.

Tx	Rx	Visibility	Bandwidth [GHz]
Omni V	Omni V	LOS	0.1, 0.2, 0.4, 1, 2, 4
15° HPBW	15° HPBW	NLOS	0.1, 0.2, 0.4, 1, 2, 4
15° HPBW	30° HPBW	NLOS	0.1, 0.2, 0.4, 1, 2, 4
15° HPBW	Omni V	NLOS	0.1, 0.2, 0.4, 1, 2, 4

The dual-polarized ultra wide-band multi-channel sounder (DP-UMCS) used in this measurements is described in [10]. This channel sounder has a 3 dB measured bandwidth (BW) of ≈ 4 GHz after calibration. The transmitter (Tx) was mounted on a static tripod pointing to the wall with an incident angle of $\approx 30°$ considering the normal to the wall. On the other side, the Rx was located on a rail pointing to the same spot in the wall, with an incident angle of $-30°$, as shown in Fig. 2. The position of the rail was adjusted with a laser pointer in such a manner that the Rx keeps focus on the same point in the wall while displacing along the rail. This is important to avoid fluctuations on the received signal of the main reflected path due to misalignment with the antenna's bore-sight.

The Rx was displaced automatically along 2.2 m in 2.5 mm steps ($\approx \lambda/2$ at 60 GHz) giving a total of 881 measurement positions. However, the spatial resolution of the channel sounder (CS) with 4 GHz BW is about 5.88 cm, meaning that there are around 24 samples in space (positions on the rail) that correspond to the same delay tap of the measured channel impulse response (CIR). This paper shows only the investigation results for Tx V and Rx V.

Table I summarizes the different bandwidths and combination of antennas that were used at the Tx and Rx.

B. Pre-pocessing of the Measurements

Each CIR was measured with a 4 GHz BW and then decimated to the target bandwidths summarized in Table I. Later, the noise floor (NF) was estimated using the same procedure as indicated in [11]. All the samples in each CIR that were lower than the NF plus a threshold of 6 dB were set to zero, as well as the samples that were lower than the maximum minus a dynamic range of 30 dB.

C. Small-scale Fading Analysis

The measured CIR at each time instance t corresponding to the position $k \in \{1 \dots 881\}$ on the rail can be represented as the sum of multiple paths arriving at the Rx in different delays τ,

$$h(t,\tau) = \sum_{\tau} \alpha_\tau e^{j\Phi_\tau} \delta(t-\tau), \quad (1)$$

where $\alpha_\tau e^{j\Phi_\tau}$ is the complex channel coefficient at the delay time τ. The normalized signal envelope $y(t)$ is calculated as

Figure 3. Picture of the measurement set-up.

the summation of the absolute value of the measured CIR in the delay domain,

$$y(t) = \frac{1}{\sqrt{\sum_{\forall t}\sum_{\forall \tau}|h(t,\tau)|^2}} \sum_{\forall \tau}|h(t,\tau)|. \tag{2}$$

The presence of a strong dominant component within other weak paths can be modelled with a Rician distribution. The Rician probability distribution function (PDF) is defined as

$$p_X(x) = \frac{x}{\sigma_n^2} e^{-\frac{x^2+A^2}{2\sigma_n}} I_0\left(\frac{A\cdot x}{\sigma_n^2}\right), \tag{3}$$

where $I_0(\cdot)$ is the modified Bessel function of the first kind with zero order. The *K*-factor K is defined as the ratio between the amplitude of the dominant path A and the variance of the weak paths σ,

$$K = \frac{A^2}{2\sigma^2}, \tag{4}$$

where the values of A and σ are extracted after fitting $y(t)$ to the Rician distribution. The power delay profile (PDP) at each time instance t is calculated as,

$$\text{PDP}(t,\tau) = |h(t,\tau)|^2. \tag{5}$$

The PDP for different directivity of the antennas at the Rx position $k = 400$ (corresponding to $0.9975\,\text{m}$ on the rail) is shown in Fig. 4. The LOS component and investigated reflections on the wall are indicated. It is also interesting to see the effect of directivity on the DS of the channel, which is reduced with hight directive antennas at both ends. Fig. 4 shows the DS using a dynamic range of $20\,\text{dB}$.

The normalized total received power per time instance t (and position k on the rail) is calculated as the sum of the power in the delay domain,

$$P(t) = \frac{1}{\frac{1}{T}\sum_{\forall t}\sum_{\forall \tau}|h(t,\tau)|^2} \sum_{\forall \tau}|h(t,\tau)|^2, \tag{6}$$

where $T = 881$ is the total number of measured time instances (points on the rail). The fade depth F is defined as the variation of the signal power and is calculated as the standard deviation σ_P of $P(t)$ expressed in dB along the rail [3]. Different system performance levels can be evaluated by scaling σ_P with s,

$$F = s\sqrt{\frac{1}{T}\sum_{\forall \tau}\left(P_{\text{dB}}(t) - \overline{P_{\text{dB}}(t)}\right)}, \tag{7}$$

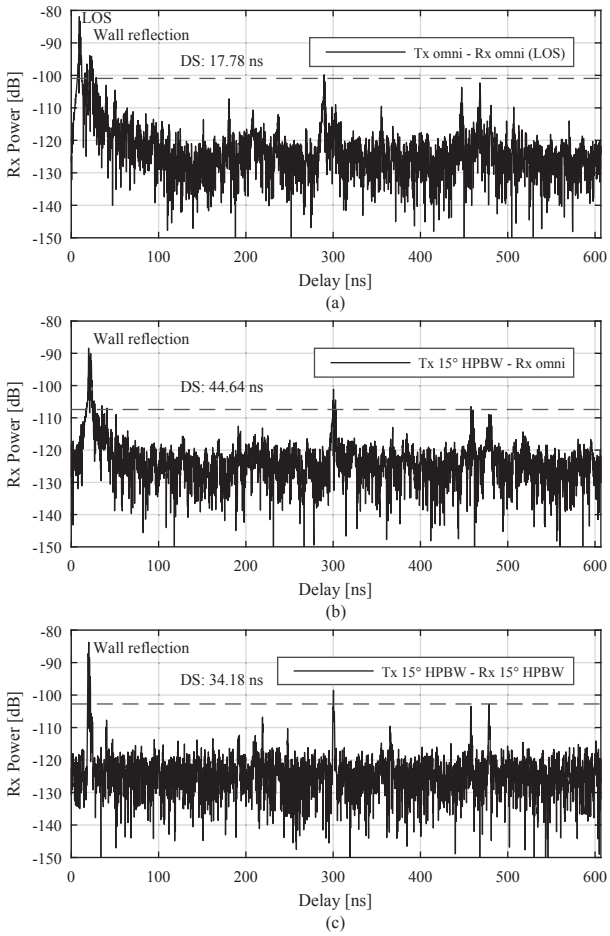

Figure 4. Measured PDP for different combinations of antennas at the position $0.9975\,\text{m}$ on the rail: (a) omni antennas at Tx and Rx with LOS component, (b) directive antenna at Tx (15° HPBW) and omni antenna at Rx, and (c) directive antennas at both ends (15° HPBW).

where $s \in \mathbb{R}$, $P_{\text{dB}}(t) = 10\log_{10}(P(t))$ and $\overline{P_{\text{dB}}(t)}$ is the mean value of $P_{\text{dB}}(t)$. Fig. 7 shows the fade depth for $s = 3$.

III. Results

A. Evolution of the Channel During Displacement

The evolution of the channel during displacement (or time) for different antennas at Tx and Rx for $4\,\text{GHz}$ BW can be observed in Fig. 5. The case of using omni antennas at both ends is shown in Fig. 5a. The LOS component can be observed and also the rising and fall of different scatterers during the

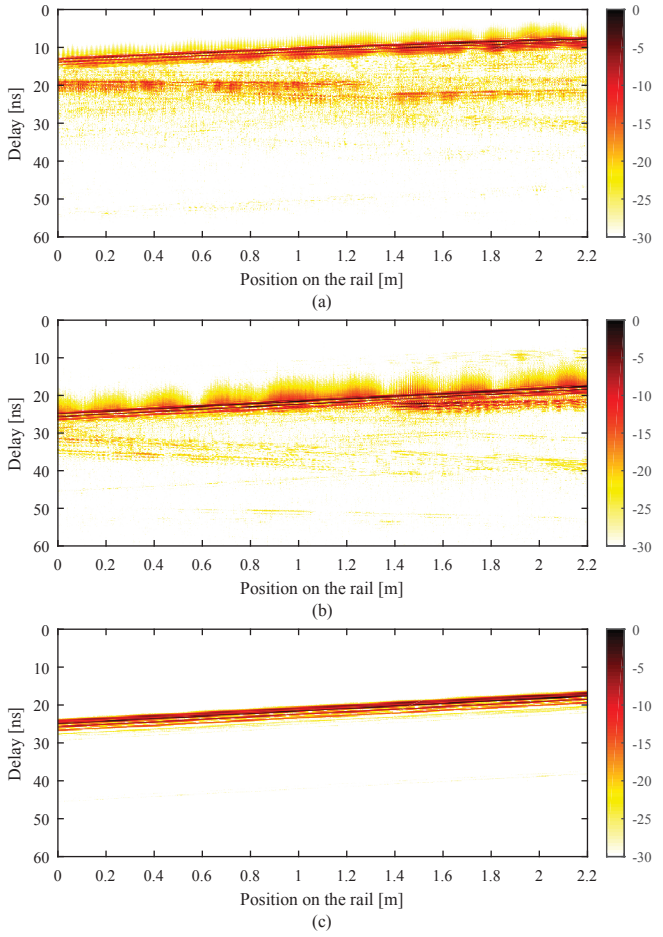

Figure 5. Normalized PDP over the distance displayed with a dynamic range of 30 dB for (a) Tx omni V and Rx omni V, (b) Tx 15° HPBW and Rx omni V, and (c) Tx 15° HPBW and Rx 15° HPBW.

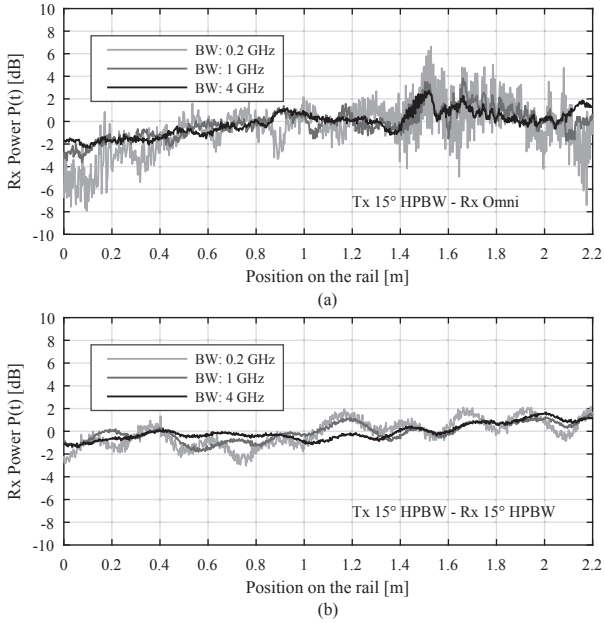

Figure 6. Received power after reflection on the wall during the displacement with (a) Tx 15° HPBW and Rx omni V, and (b) Tx 15° HPBW and Rx 15° HPBW.

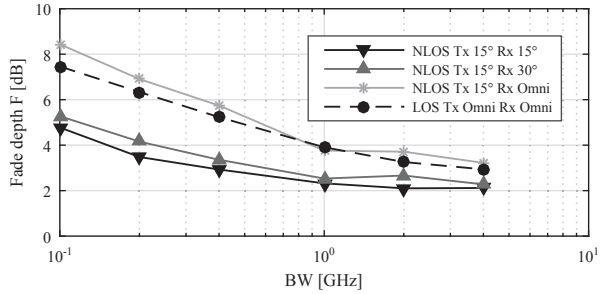

Figure 7. Fade depth for different bandwidths and directive antennas for $s = 3$.

displacement. This scenario has a relative high *K*-factor due to the strong LOS component present during all the movement. On the other hand, Fig. 5b shows the case of using a directive antenna (15° HPBW) at the Tx and omni at Rx. The numbers of multipath components is reduced compared to Fig. 6a. However, there are still strong scatterers showing up, e.g., at 1.4 m. This is also visible in Fig. 6a in which there is an increment on the received power. These multiple scatterers generate fading with reduced bandwidths (shown in Fig. 7). Finally, Fig. 5c shows the case of 15° HPBW at Tx and Rx. It can be observed that there are no other considerable scatterers than the specular reflections from the wall, and they all remain constant during displacement.

B. Influence of Bandwidth and Directivity on Fading

The received power $P(t)$ along the rail for different bandwidths and antennas is displayed in Fig. 6. It can be observed that when using low directive antennas at the Rx, Fig. 6a, the fading is increased in comparison to high directive antennas, Fig. 6b. Furthermore, a smoother line can be observed with an increasing bandwidth if we analyse the same Tx-Rx antenna combination. These results are consistent with what expected from literature and our hypothesis.

C. Fade Depth Scaling with Bandwidth and Directivity

Fig. 7 shows the observed fade depth for the different antenna combinations and bandwidths. It can be observed that there is a reduction of the fade depth not only with the bandwidth as already shown in [3], but also with the increment on the directivity of the antennas. It is interesting to notice that for the 15° HPBW at Tx and omni Rx, with shorter bandwidth the fade depth is increased considerable in comparison to the 15° HPBW Rx antenna.

D. K-factor Analysis

Table II summarizes the estimated *K*-factors. The empirical cumulative distribution function (CDF) of the signal level for the Tx omni and Rx omni case and different bandwidths can be seen in Fig. 8. With an increasing bandwidth, the variation of received signal is lower compared to the mean, indicating a small fade and a large *K*-factor. On the other hand,

Table II
K-FACTOR AT DIFFERENT BANDWIDTHS AND WITH DIFFERENT ANTENNA COMBINATIONS.

	Visibility	0.1 GHz	0.2 GHz	0.4 GHz	1 GHz	2 GHz	4 GHz
omni/omni	LOS	6.15 dB	8.45 dB	11.31 dB	16.30 dB	17.61 dB	17.65 dB
15°/omni	NLOS	3.92 dB	6.72 dB	8.77 dB	12.55 dB	12.52 dB	12.40 dB
15°/30°	NLOS	7.24 dB	11.27 dB	13.89 dB	18.26 dB	17.85 dB	18.02 dB
15°/15°	NLOS	7.27 dB	12.93 dB	15.05 dB	18.50 dB	17.74 dB	18.25 dB

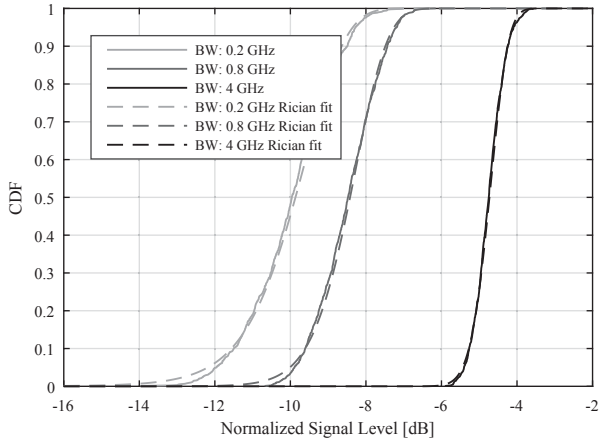

Figure 8. Normalized received signal level during the displacement for different BW in the Tx omni and Rx omni combination.

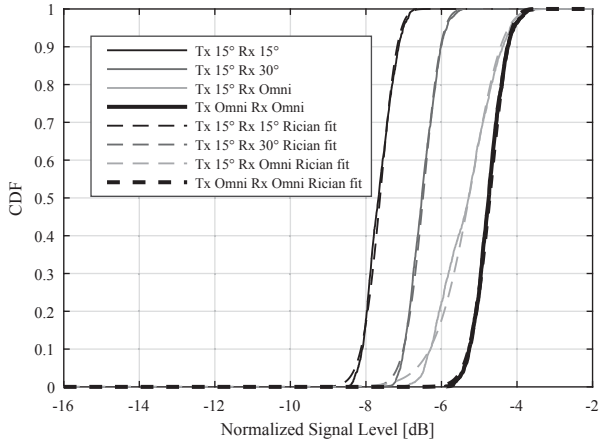

Figure 9. Normalized received signal level during the displacement for 4 GHz BW and different combination of antenna directivity at Tx and Rx.

Fig. 9 shows the CDF of the signal for the same bandwidth, but different directivity on the antennas. It also results in an increment on the K-factor with an increasing directivity in the NLOS scenario.

IV. Conclusions

Fading measurements of a scattering process at 60 GHz have been performed in an indoor scenario using different directive antennas and bandwidths aiming to investigate the relation between directivity, bandwidth, and fading. The emulation of a beam-former pointing to a scatterer shows that the NLOS beam behaves quasi-deterministic with a high K-factor. Furthermore, the influence of bandwidth and directivity was also analysed, showing that with larger bandwidths the fade depth is reduced. The same happens with increasing directivity.

Large K-factors in reflections using directive antennas and large bandwidths show the presence of strong deterministic components. This supports the implementation of quasi-deterministic channel models, in which some of the scatterers are treated as deterministic paths, contrary to traditional SCM in which only the LOS component has a deterministic approach.

References

[1] D. Dupleich, F. Fuschini, R. Mueller, E. Vitucci, C. Schneider, V. Degli Esposti, and R. S. Thomae, "Directional characterization of the 60 GHz indoor-office channel," in *2014 XXXIth URSI General Assembly and Scientific Symposium (URSI GASS)*, pp. 1–4.

[2] D. Dupleich, S. Haefner, C. Schneider, R. Mueller, R. S. Thoma, J. Luo, E. Schulz, X. Lu, and G. Wang, "Double-Directional and Dual-Polarimetric Indoor Measurements at 70 GHz," *2015 IEEE 26th International Symposium on Personal Indoor and Mobile Radio Communications (PIMRC)*, 2015.

[3] B. Allen, W. Q. Malik, and D. J. Edwards, "Bandwidth-dependent modelling of small-scale fade depth in wireless channels," *IET Microwaves, Antennas & Propagation*, vol. 2, no. 6, pp. 519–528, 2008.

[4] P. Kyosti et al., "WINNER II Channel Models: IST-4-027756 WINNER II D1.1.2 V1.1," 2007. [Online]. Available: www.ist-winner.org/WINNER2-Deliverables/D1.1.2v1.1.pdf

[5] L. Liu, C. Oestges, J. Poutanen, K. Haneda, P. Vainikainen, F. Quitin, F. Tufvesson, and P. Doncker, "The COST 2100 MIMO channel model," *IEEE Wireless Communications*, vol. 19, no. 6, pp. 92–99, 2012.

[6] V. Nurmela, A. Karttunen, A. Roivainen, L. Raschkowski, T. Imai, J. Jarvelainen, J. Medbo, J. Vihriala, J. Meinila, K. Haneda, V. Hovinen, J. Ylitalo, N. Omaki, K. Kusume, P. Kyosti, T. Jamsa, A. Hekkala, R. Weiler, and M. Peter, "METIS Channel Models: Deliverable D1.4," 2015.

[7] M. K. Samimi, G. R. MacCartney, S. Sun, and T. S. Rappaport, "28 GHz Millimeter-Wave Ultrawideband Small-Scale Fading Models in Wireless Channels," in *2016 IEEE 83rd Vehicular Technology Conference (VTC Spring)*, pp. 1–6.

[8] R. J. Weiler, M. Peter, W. Keusgen, A. Maltsev, I. Karls, A. Pudeyev, I. Bolotin, I. Siaud, and A.-M. Ulmer-Moll, "Quasi-deterministic millimeter-wave channel models in MiWEBA," *EURASIP Journal on Wireless Communications and Networking*, vol. 2016, no. 1, p. 74, 2016.

[9] N. Iqbal, C. Schneider, J. Luo, D. Dupleich, R. Müller, S. Haefner, and R. S. Thomä, "On the Stochastic and Deterministic Behavior of mmWave Channels," in *The 11th European Conference on Antennas and Propagation (EuCAP 2017) (EuCAP 2017)*, Paris, France, 2017.

[10] R. Mueller, R. Herrmann, D. A. Dupleich, C. Schneider, and R. S. Thomae, "Ultrawideband multichannel sounding for mm-wave," in *2014 8th European Conference on Antennas and Propagation (EuCAP)*, pp. 817–821.

[11] A. Bottcher, C. Schneider, P. Vary, and R. S. Thomae, "Dependency of the power and delay domain parameters on antenna height and distance in urban macro cell," in *Antennas and Propagation (EUCAP), Proceedings of the 5th European Conference on*, 2011, pp. 1395–1399.